



Influences of puff protocols and upper airway anatomy on cannabis pharmacokinetics: A CFPD-PK study

Jianan Zhao^{a,b}, Yu Feng^{a,*}, Geng Tian^{b,**}, Cassandra Taylor^b, N. Sarah Arden^b

^a School of Chemical Engineering, Oklahoma State University, USA

^b Office of Pharmaceutical Quality, Center for Drug Evaluation Research, US Food and Drug Administration, USA

ARTICLE INFO

Keywords:

Computational fluid particle dynamics (CFPD)
Pharmacokinetics (PK)
Cannabis
Δ9-tetrahydrocannabinol (THC)
Smoking
Vaping

ABSTRACT

Predicting the optimal administration doses of the inhaled Δ9-tetrahydrocannabinol (THC), i.e., one of the major natural compounds in cannabis, is critical for maximizing the therapeutic outcomes and minimizing the toxic side effects. Thus, it is essential to developing an aerosol dosimetry model to simulate the transport, deposition, and translocation of inhaled THC aerosols from the human respiratory system to the systemic region. In this study, a computational fluid-particle dynamics (CFPD) plus pharmacokinetics (PK) model was developed and validated to quantify the localized vapor and particle uptake rates of THC and the resultant THC-plasma concentrations using two human upper airway geometries. In addition, two different puff protocols (4.0/10.0 s and 1.6/11.4 s as the inhalation/holding time ratios) were employed, associated with two different inhaled THC doses (2.0 mg and 8.82 mg, respectively). The computational results demonstrated that multiple parameters had noticeable influences on THC particle deposition and vapor absorption in the upper airways, as well as the resultant pharmacokinetic behaviors. These factors include anatomical features of the upper airway, puff flow rate, duration, and holding time. The results indicated that puff protocol with 4.0/10.0 s inhalation/holding time ratio would be recommended if the treatment needs THC delivery to the deeper lung. Furthermore, the inhaled THC dose had a dominant effect on the THC-plasma PK profiles, which could override the influences of anatomical variability and puff protocols. The developed CFPD-PK modeling framework has the potential to provide localized lung absorption data and PK profiles for *in vitro-in vivo* correlation, as well as supporting the development and assessment of drug products containing cannabis or cannabis-derived compounds.

1. Introduction

The plant *Cannabis sativa* L. (i.e., the family Cannabaceae) is known to contain over 100 different naturally occurring compounds (e.g., cannabinoids, terpenes, and other phytochemicals). One of the most well-known cannabinoids is Δ9-tetrahydrocannabinol (THC). Δ9-THC is considered the major psychoactive intoxicating component of cannabis (i.e., the component responsible for the "high" people may experience from using cannabis). The use of cannabis in mainstream products has exponentially grown in popularity over the past decade [1]. Since 2012, the sale of cannabis for adult recreational use has been legalized in nine states in the US [2]. Cannabis can be consumed in various ways. The most popular routes of administration (ROAs) are inhalation (e.g., smoked and vaporized) and oral (e.g., capsules, tinctures, and edibles). Approximately 90% of Δ9-THC in the blood circulates in plasma and is

sequestered mainly in red blood cells [3]. Being administered *via* inhalation through the pulmonary route, Δ9-THC is detected in plasma within seconds after the first puff of a cannabis cigarette and the peak plasma concentration is achieved within 3–10 min [3]. The bioavailability and pharmacokinetics (PKs) of the Δ9-THC are directly related to the deposition sites of the inhaled cannabis particulate and vapor phases in the human respiratory system and the subsequent translocation into the blood circulation [4]. Furthermore, the bioavailability of Δ9-THC can be significantly influenced by the puff protocol, i.e., puff volume, puff duration, as well as the holding time after each puff [5]. Specifically, the puff protocol and puff volume influence the degree of Δ9-THC exposure. Systemic bioavailability generally ranges from 10% to 50% [6,7]. Based on the fact that 30% of Δ9-THC can be decomposed by pyrolysis, the systemic bioavailability of Δ9-THC is about 25% for heavy users and 10–14% for occasional users [8,9]. Since this study focuses on

* Corresponding author. 420 Engineering North, Stillwater, OK, 74078, USA.

** Corresponding author. 10903 New Hampshire Ave, Silver Spring, MD, 20993, USA.

E-mail addresses: yu.feng@okstate.edu (Y. Feng), geng.tian@fda.hhs.gov (G. Tian).

the research of $\Delta 9$ -THC, the THC in the paper represents $\Delta 9$ -THC only.

Historically, smoking has been the preferred ROA for cannabis over the oral route due to the relatively higher bioavailability and the public access to cannabis raw materials used in smoking. More recently, vaping cannabis raw material has increased in popularity, and many more oral products have become available in the marketplace [10]. However, smoking-type cannabis is known to be harmful to the human body due to the hazardous combustion products formed from high temperatures, such as tar, carbon monoxide and other carcinogens, generated during smoking [11]. Hence, cannabis vaping has drawn more attention as an alternative ROA for cannabis raw material. As a non-pyrolytic method (the temperature at approximately 200 °C), the vaporization of cannabis may be a promising strategy to reduce the side effects of cannabis combustion and smoking [12]. Clinical tests of cannabis also suggest higher bioavailability of vaping than smoking [10]. Considering that inhalation pattern differences may influence the absorption of $\Delta 9$ -THC by users, different puff protocols were employed in this study to investigate the effect of inhalation patterns on the PKs of cannabinoids.

The relationships between PK of THC and inter-subject variability according to gender, age, the frequency of use, and the known amounts of THC in cannabis raw material used for creating cigarettes have been explored in previous studies [13–15]. The research results show that heavy smokers tend to draw a deeper inhalation with a higher puff volume and shorter puff duration, and the variation of PK of THC among different individuals indicates there is a relationship between THC absorption rate and airway morphological features. Other researchers [5] investigated cannabis puff protocol (puff volume and breath-holding time) effects on the biological exposure, and the results indicated that the THC concentration in plasma was closely related to the puff volume and the holding duration between two consecutive puffs. The effect of breath-holding on THC concentration in plasma was apparent when higher potency (3.55% vs. 0.8%) cannabis cigarettes were used, as 3.55% THC was considered as “high potency” 25 years ago [16].

Currently, there are no benchmark investigation tools to quantitatively predict the optimal THC doses to maximize the therapeutic outcomes and minimize the toxic side effects. Integrating clinical data such as plasma THC concentration ($C_{\text{THC-plasma}}$) vs. time, computational models are potentially valuable tools to gain a better understanding of the PK of cannabinoids in the human body, and may provide high-resolution quantitative evidence for cannabis regulation and medication development in the future. Existing modeling efforts have been made using only PK models [17–19]. Experimentally validated PK models are capable of predicting the real-time concentration profiles, the corresponding maximum plasma concentration C_{max} at time t_{max} , the area under the curve (AUC), and the derived bioavailability and half-life. The above-mentioned data can be used for dosing optimization to achieve a favorable clinical outcome by considering the clinically relevant features of specific patients and for clinical trial design.

Specifically, two-compartment and three-compartment models were developed and optimized by Liu and Martin, matching the time course of plasma concentrations of cannabinoids [20]. Another PK model was developed with more than three compartments to obtain better fits to the THC-plasma concentration time course in animal studies [21]. Hunault, van Eijkeren, Mensinga, de Vries, Leenders and Meulenbelt [19] formulated a three-compartment PK model for predicting THC plasma concentration by fitting to the clinical data obtained from naïve and mild cannabis users, focusing only on the administration *via* smoking. Heuberger, Guan, Oyetayo, Klumpers, Morrison, Beumer, van Gerven, Cohen and Freijer [17] developed an integrated population PK model applicable to multiple administration routes, such as oral and pulmonary routes. The PK model was built based on the traditional three-compartment model with one peripheral compartment accounting for the slow release backflow to the central compartment.

However, employing the PK models requires the simplification of lung dosage estimation without accurate local and regional deposition and absorption data. In addition, the effects of puff protocols and subject

variabilities on the lung delivered doses *via* smoking/vaping have not been considered. To fill the gap and investigate the effects of puff protocols and subject variability on THC lung deposition and THC-plasma levels, this study quantitatively evaluated the THC PKs by developing a multiscale Computational Fluid-Particle Dynamics plus Pharmacokinetic (CFPD-PK) model. CFPD models have been employed for decades to investigate particle-laden airflow transport phenomena in human respiratory systems [22–29]. The integration of the CFPD-informed results into the PK model provides a more realistic approach over the traditional techniques [30,31]. Specifically, CFPD-PK modeling capabilities enable the explicit simulation of the transport of continuous THC vapor phase and discrete particle phase in the respiratory system, as the inputs to the PK model, which are coupled in tandem. Employing two upper airway configurations from mouth to generation 3 (G3) of the airways (see Fig. 1), this study simulated and compared the THC deposition, absorption, and translocation in the virtual human body. For safety risk and therapeutic effect evaluations, the local and regional deposition and absorption patterns, THC-plasma concentrations associated with different puff protocols, and airway morphologies were compared. For a broader impact, the development of this coupled CFPD-PK modeling framework can be easily extended for the estimation of the transport and translocation of other chemical compounds, starting from the inhalation *via* the pulmonary route. To the best of our knowledge, although CFPD-PK models have been developed for many inhaled drugs and toxicants, this study is the first numerical modeling effort to develop such a multiscale model for THC.

2. Methodology

2.1. Upper airway geometries and meshes

To investigate the effect of the upper airway anatomy on THC fates in lung and systemic region, two upper airway geometries were employed for the CFPD predictions of the transport/deposition/absorption of THC particle and vapor, *i.e.*, an idealized upper airway geometry (see Fig. 1 (a)) [32] and an “elliptical” Virginia Commonwealth University (VCU) upper airway geometry (see Fig. 1 (b)) [33,34]. Both geometries were reconstructed with an 8.0 mm-diameter circular mouth-opening as the inlet of the THC and airflow. The coordinates of the inlet centers are both (0, 0, 0). Due to the importance of the mucociliary clearance and the physiological characteristics of the respiratory system [35] regarding THC absorption by the lung, this study defined a local bioavailability coefficient [26] of THC, $F_{i,\text{phase}}$, to account for the removed proportion of the delivered dose from the lungs by mucus clearance [35] and the difference in THC absorption in different lung regions are physiologically real, which is resulted from varying lung surfactant, surface lining fluid, the thickness of epithelium etc., through the upper airway tract [36]. In addition, to consider different mucus thicknesses and the presence of the lymph veins connected with the sub-epithelium layers in different portions of the lung [37], the airway domains were divided into four regions, *i.e.*, R1 to R4 (see Fig. 1). Each region has specific bioavailability coefficients for the particle phase ($F_{i,p}$) and vapor phase ($F_{i,v}$). As shown in Fig. 1, Region 1 (R1) contains the oral cavity and pharynx with the thickest mucus layer and lowest lymph vein concentration. Region 2 (R2) contains the trachea with a thinner mucus layer and higher numbers of lymph veins connected to the tissue compared with Regions 1. Region 3 (R3) consists of the tracheobronchial tree from G1 to G3. Region 4 (R4) represents the airways beyond G3, which is not included in the geometry. In this study, it is assumed that the THC entering Region 4 can be 100% absorbed.

The idealized upper airway geometry (see Fig. 1 (a)) was meshed with the hexahedral element by ICEM CFD 18.0 (Ansys Inc., Canonsburg, PA). The structured, multi-block hexahedral meshes were refined at the wall boundaries with six prism layers to resolve the velocity gradient near the wall. The final mesh contains 3,594,881 cells and 3,675,308 nodes. To prove that the simulation results were independent

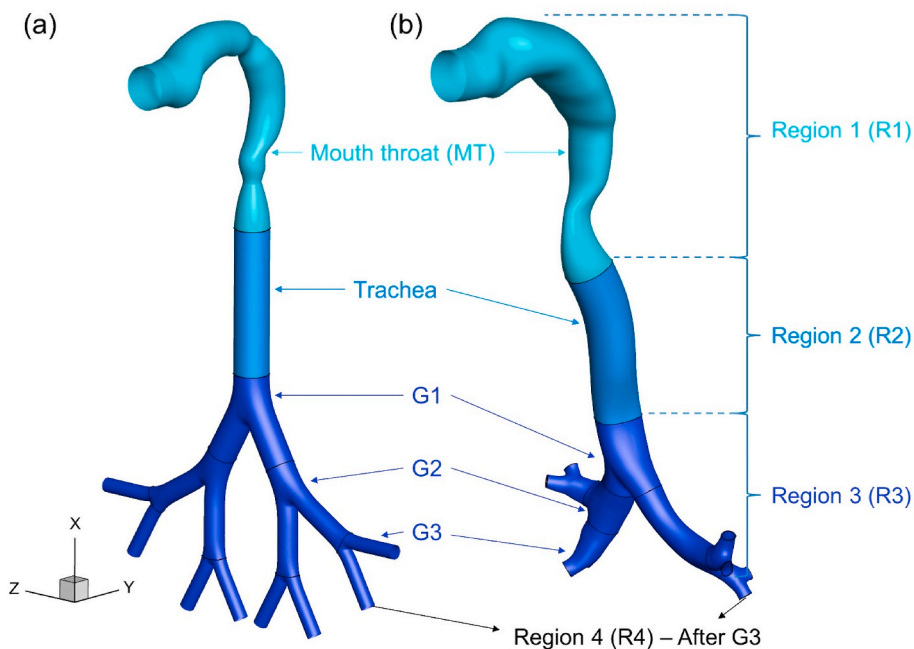


Fig. 1. Upper airway geometries employed for CFPD simulation: (a) idealized upper airway and (b) elliptical VCU airway models.

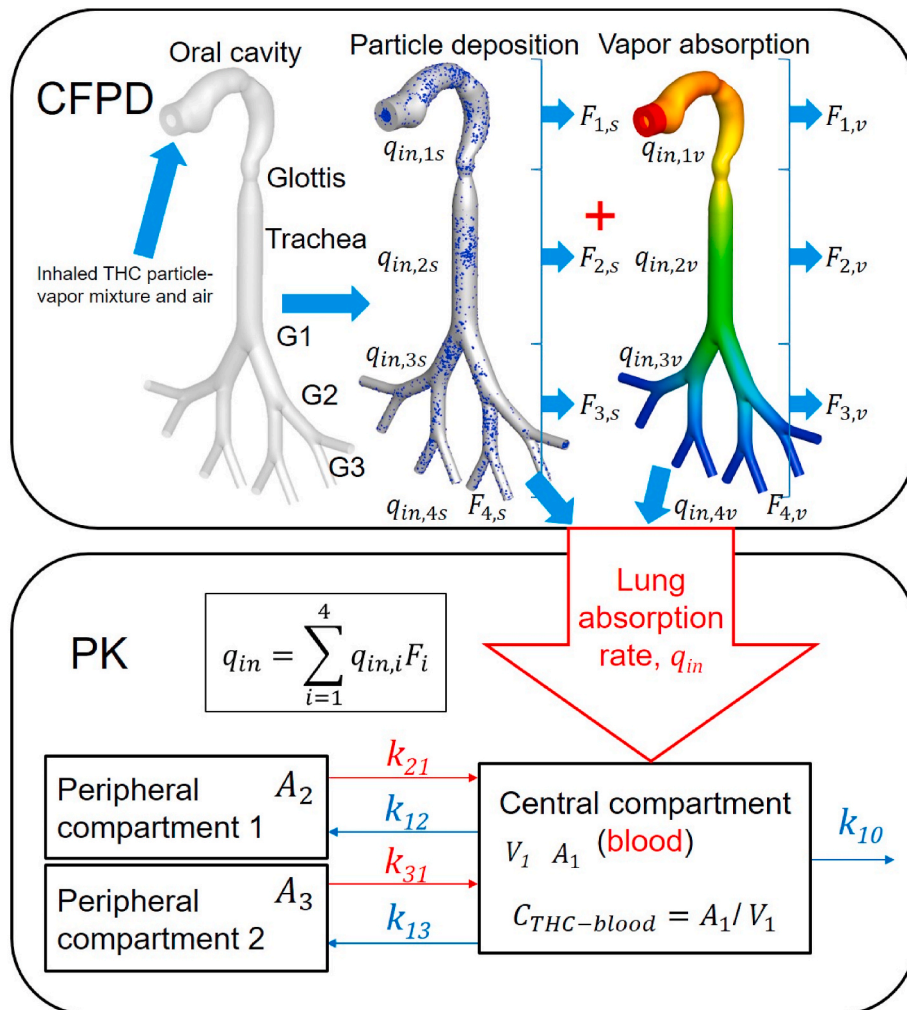


Fig. 2. Framework of the multiscale CFPD-PK model with the color map representing the local vapor absorption rate at airway walls.

of further mesh refinement from the final mesh, the mesh independence test was performed in [31] with the inlet volumetric flow rate of 27.5 mL/s. Furthermore, the final mesh of the elliptical VCU geometry (see Fig. 1 (b)) contains 516,880 structured hexahedral cells and 541,992 nodes, based on the mesh independence test done for laminar flow.

2.2. Governing equations

This study assumed that both particle and vapor phases of THC were generated during smoking or vaping [38]. Hence, the Newton's second law of motion and convection-diffusion equations were employed to predict the particle and vapor dynamics in the airways, respectively. The CFPD-PK model is a promising multiscale model for predicting regional deposition and absorption of smoked and vaporized cannabis under different puff protocols and dosing scenarios, as well as bioavailability and pharmacokinetics (PKs) of chemical compounds [31,39]. The schematic of the CFPD-PK modeling framework is shown in Fig. 2. Specifically, the CFPD model takes the puff protocol information (see Tables 2 and 3) as the inputs for the model and predicts the transport and absorption rate of both vapor and solid phases of the THC as the output results. Then, the PK model uses the THC absorption rate by the lung as the input to predict the THC plasma level varying with time.

2.2.1. Computational fluid-particle dynamics (CFPD)

2.2.1.1. Continuous phase. Due to the low puffing flow rates ranging from 20 to 45 mL/s for typical cannabis smoking [5,15,40], the highest Reynolds number Re in the entire upper airway domain is less than 1,000, indicating that the airflow regime in the entire computational domain remains laminar. Additionally, since the temperature and pressure variations during the puffing process are small, the air-THC vapor mixture is considered as an incompressible Newtonian fluid. Thus, the conservation laws for the air-vapor mixture calculation are

$$\frac{\partial u_i}{\partial x_i} = 0 \quad (1)$$

$$\rho \left(\frac{\partial u_i}{\partial t} + u_j \frac{\partial u_i}{\partial x_j} \right) = - \frac{\partial p}{\partial x_i} + \mu \frac{\partial^2 u_i}{\partial x_j^2} + \rho g_i \quad (2)$$

where ρ is the density of the air-vapor mixture, u_i represents the fluid velocity component in the i -direction, $g_i = (-9.81, 0, 0) \text{ m/s}^2$ is the gravitational acceleration (see Figs. 1 (a) and (b) for the coordinate system), p is the pressure, and μ is the dynamic viscosity of the air-vapor mixture.

The energy transport equation can be written as

$$\rho C_p \left(\frac{\partial T}{\partial t} + u_i \frac{\partial T}{\partial x_i} \right) = k \nabla^2 T + \mu \Phi_T \quad (3)$$

where T is the temperature, k is the thermal conductivity, C_p is the specific heat of the air-vapor mixture at constant pressure, and $\mu \Phi_T$ stands for the rate of mechanical energy into internal energy per unit volume by viscous dissipation. In this study, it is assumed that the C_p of the mixture is equal to the specific heat of air due to the low fraction of the vapor THC in air (less than 2%).

In addition, the vapor phase is modeled as transported species, which can be described using species mass transport equation (Eq. (5)),

$$\frac{\partial Y_{\text{THC}}}{\partial t} + u_j \frac{\partial Y_{\text{THC}}}{\partial x_j} = \frac{\partial}{\partial x_j} \left(\tilde{D}_{\text{THC-air}} \frac{\partial Y_{\text{THC}}}{\partial x_j} \right) \quad (4)$$

where Y_{THC} is the mass fraction of the vapor THC and $\tilde{D}_{\text{THC-air}}$ is the vapor THC molecular diffusivity of vapor phase in air, which is estimated using Eq. (5), *i.e.*,

$$\tilde{D}_{\text{THC-air}} = \frac{T^{1.75} (1/M_{\text{THC}} + 1/M_{\text{air}})^{1/2}}{p \left(v_{\text{THC}}^{1/3} + v_{\text{air}}^{1/3} \right)^2} \times 10^{-3} \quad (5)$$

in which M 's are the molecular weight for THC and air in g/mol, T is the temperature in K, and p is the pressure in atm, and v 's are dimensionless diffusion volumes [41,42]. The calculation of v 's is documented in Ref. [42]. At standard temperature and pressure, $\tilde{D}_{\text{THC-air}}$ has a value of $1.43 \times 10^{-1} \text{ cm}^2/\text{s}$.

2.2.1.2. Particle phase. Because of the low volume fraction of the THC carried by air, the trajectory of THC particles was calculated using the one-way Euler-Lagrange approach [26,43], which neglected the interactions between particles. The translational motion of each particle is individually calculated by integrating the force balance on the particle to determine the particle velocity u_i^p and position x_i^p . The force balance for each particle can be given by

$$\frac{dx_i^p}{dt} = u_i^p \quad (6)$$

$$m_p \frac{d}{dt} (u_i^p) = F_i^D + F_i^L + F_i^{BM} + F_i^G \quad (7)$$

In which m_p is the particle mass, F_i^D represents the drag force [25,44], F_i^G is the gravitational force, F_i^{BM} is the Brownian motion induced force [23,45], and F_i^L is the Saffman lift force [46]. The particle time step is estimated based on the work done in [43] with an expression

$$\Delta t_p = \frac{C_c m_p}{3\pi\mu d_p} \quad (8)$$

where m_p is the particle mass, d_p is the particle diameter, μ is the dynamic viscosity of air, and C_c is the Cunningham slip correction factor, which can be calculated as [47].

$$C_c = 1 + \frac{2\lambda}{d_p} \left[1.257 + 0.4 \exp \left(-0.55 \frac{d_p}{\lambda} \right) \right] \quad (9)$$

In Eq. (9), λ is the mean free path of air, which can be calculated by

$$\lambda = \lambda_0 \left(\frac{T}{T_0} \right) \left(\frac{P_0}{P} \right) \left(\frac{1 + \frac{S}{T_0}}{1 + \frac{S}{T}} \right) \quad (10)$$

where $\lambda_0 = 0.0673 \text{ }\mu\text{m}$, $P_0 = 760 \text{ mmHg}$, $T_0 = 296.15 \text{ K}$, and $S = 110.4 \text{ K}$ [48].

2.2.2. Boundary conditions for the CFPD model

The puffing boundary conditions are extracted from the users' data of Volcano® Medic vaporizer, which is one of the popular types of devices for cannabis vaporizing [10,13,17]. Specifically, vapor and particle mass fractions regarding total THC dose are 58.4% and 25.0%, respectively, whereas the rest is considered lost during the vaporization process [11]. The mass fractions mentioned above were used to calculate the inlet partitions between the vapor and particle phases of the inhaled THC.

Both monodispersed and polydispersed THC particle size distributions (PSDs) are used as the inlet conditions in order to evaluate whether using monodispersed PSD with the mass median aerodynamic diameter (MMAD) of the realistic polydispersed PSD is an eligible simplification to reduce the computational cost of the CFPD simulations with negligible differences in THC fate predictions. Specifically, PSDs employed at the injection location, *i.e.*, the mouth inlet, are shown in Fig. 3. Specifically, for the monodisperse case (see Fig. 3 (a)), the particle diameter is assumed as 450 nm (the MMAD of the realistic polydispersed PSD), and

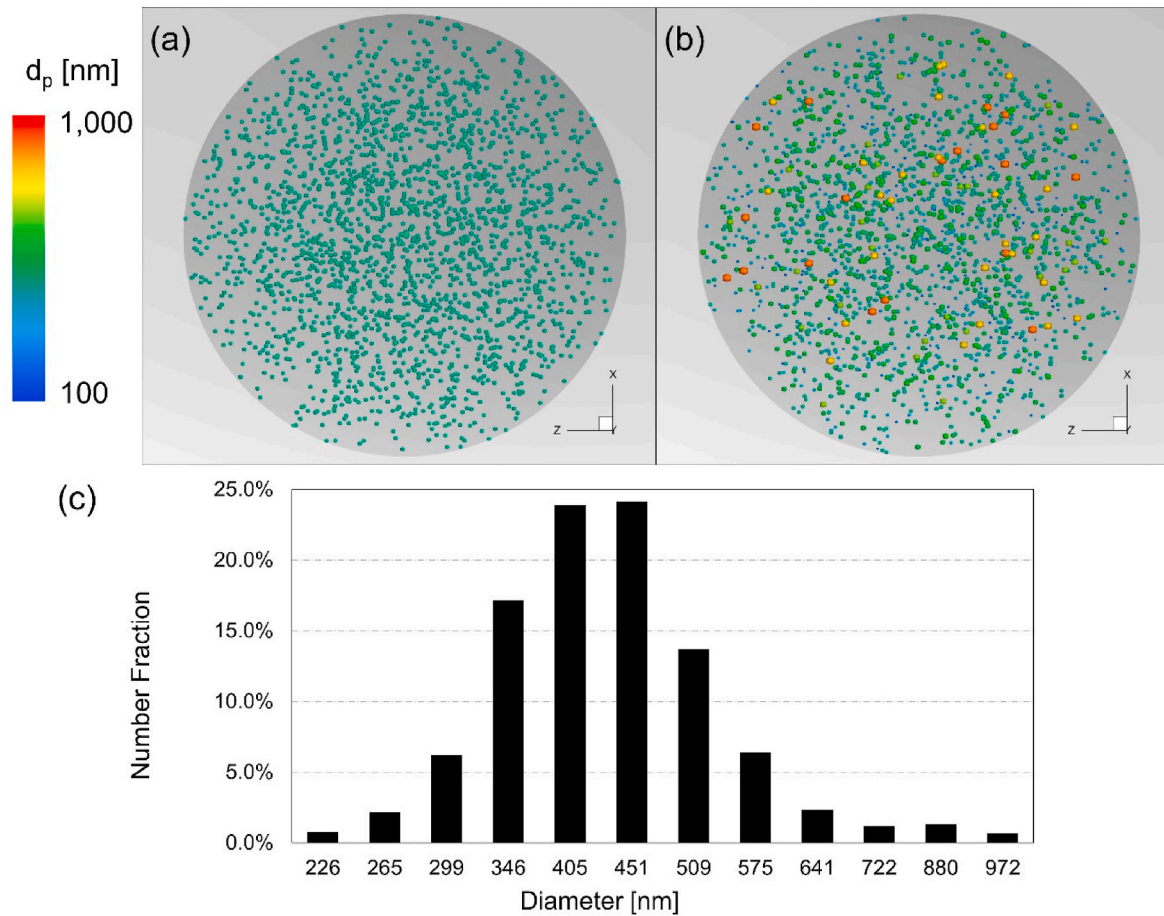


Fig. 3. Particle size distribution at mouth inlet: (a) monodisperse and (b) polydisperse, and (c) particle number fraction distribution for the polydisperse cases.

the realistic polydispersed PSD (see Fig. 3 (b) and (c)) is based on the work by Hiller et al. [49]. Particles and vapor are released at the beginning of the puff at the mouth. Particles are considered as “deposited” when the distance between the center of the spherical particle and the airway wall is equal to or less than $d_p/2$. The regional deposition of particles in upper airways can be quantified by the regional deposition fraction (RDF), which is defined as [43]

$$RDF = \frac{\text{Number of deposited particles in a specific region}}{\text{Number of particles entering the mouth}} \quad (11)$$

As one puff breath is fast with a typical range from 1.6 s to 4.8 s [5, 14], it is reasonable to assume that the THC vapor phase is nonreactive during the transport and absorption processes in the human lung. Also, we assume that the THC vapor concentrations at both sides of the air-mucus interface are in equilibrium and always satisfy Henry’s law. Due to the lipophilic characteristics of the THC ($\log K_{ow} = 6.97$ [50]), the vapor molecules are rapidly removed through the tissue. Hence, the vapor concentration in the tissue is assumed to be always equal to zero [32]. The 3rd-type boundary condition can be employed at the airway walls for vapor absorption using

$$\frac{\partial Y_{THC,v}}{\partial n} \Big|_{n=0} + \Gamma_{THC,w} \cdot Y_{THC,v} \Big|_{n=0} = 0 \quad (12)$$

where $\Gamma_{THC,w} = 7.06 \times 10^4 \text{ m}^{-1}$ is the absorption coefficient of the THC through the airway wall. Details about the calculation of the wall absorption coefficient can be found in Feng et al. [32]. In this study, the mucus thickness is assumed to be $10 \mu\text{m}$ [51]. Based on the work by Ref. [52], the THC vapor diffusivity in the mucus phase is estimated as $3.23 \times 10^{-5} \text{ cm}^2/\text{s}$. The dimensionless gas-liquid equilibrium partition

coefficient (i.e., dimensionless Henry’s law constant) for THC vapor is estimated to be 4.47×10^{-7} (data source: <http://satellite.mpic.de/henry/>). Assuming that the deposition rate of THC vapor phase at the airways wall is as high as infinite, the boundary condition at the wall is $Y_{wall} = 0$. Hence, the overall mass fraction gradient at the wall can be evaluated as

$$\frac{\partial Y_{THC,v}}{\partial n} \Big|_w = \frac{Y_{THC,v} \Big|_c - Y_{THC,v} \Big|_w}{0.5h_{cell}} = \Gamma_{THC,w} \cdot Y_{THC,v} \Big|_w \quad (13)$$

where $Y_{THC,v} \Big|_c$ is the mass fraction at the center of the near-wall mesh cell, $Y_{THC,v} \Big|_w$ is the mass fraction at the mesh wall surface, and h_{cell} is the height of the near-wall prism layer. Therefore, the overall absorption mass flow rate can be expressed as

$$\dot{m}_{THC,wall} = \sum_{i=1}^n j_{THC,i} S_i \quad (14)$$

In Eq. (14), S_i is the wall surface area of the i -th cell and $j_{THC,i}$ is the wall mass flux of THC vapor at the i -th wall surface cell, which can be given by

$$j_{THC,i} = \rho_{a-THC} \tilde{D}_{THC-air} \Gamma_{THC,w} \cdot Y_{THC,v} \Big|_w \quad (15)$$

To evaluate the regional vapor uptake, the absorption fraction (AF) of the THC vapor phase is introduced which can be defined as

$$AF_i = \frac{\dot{m}_{THC,wall}}{\dot{m}_{THC,v,total}} \quad (16)$$

where $\dot{m}_{THC,v,total}$ is the vapor-mass flow rate entering the mouth inlet.

2.2.3. Pharmacokinetic (PK) model

A three-compartment PK model has been developed and validated with clinical data to be able to quantitatively predict the THC-plasma concentration ($C_{\text{THC-plasma}}$) [17]. The schematic of the three-compartment model is shown in Fig. 2. Specifically, the PK model has one central compartment and two peripheral compartments. In this study, the lung tissue metabolism of THC is assumed to be negligible [3]. The PK model validations can be found in Section 3.1. For the prediction of the $C_{\text{THC-plasma}}$ vs. time, the governing equations of the PK model are

$$\frac{dA_1}{dt} = q_{\text{in}} - k_{12}A_1 - k_{13}A_1 - k_{10}A_1 + k_{21}A_2 + k_{31}A_3 \quad (17)$$

$$\frac{dA_2}{dt} = k_{12}A_1 - k_{21}A_2 \quad (18)$$

$$\frac{dA_3}{dt} = k_{13}A_1 - k_{31}A_3 \quad (19)$$

$$C_{\text{THC-plasma}} = A_1/V_1 \quad (20)$$

where A_i represent the total mass of THC in i^{th} compartment, q_{in} is the instantaneous THC absorption rate via inhalation, and k_{ij} represent the transfer rate constant of THC from compartment i to j ($i, j = 1, 2, \text{ or } 3$). Furthermore, k_{10} is the elimination rate of THC from the central compartment ($i = 1$). $C_{\text{THC-plasma}}$ is the THC-plasma concentration, and V_1 is the volume of the central compartment ($i = 1$).

2.3. Numerical setup

Ansys Fluent 19.2 (Ansys Inc., Canonsburg, PA) was used to run the CFPD-PK model. Specifically, the PK modeling is achieved via in-house C programs as user-defined functions (UDFs). The equations were discretized using the finite volume method and 2nd-order schemes in both time and space. To ensure the numerical stability, the flow time step employed was 0.05 s [31]. Particle time step (see Eq. (8)) ranges from 2.9e-7 to 3.5e-6 s. Convergence was considered achieved when all residuals became lower than 1.0e-5. Numerical simulations were performed on a local Dell Precision T7810 workstation (Intel® Xeon® Processor E5-2643 v4 with dual processors, 64 cores and 128 GB RAM) and a local Dell Precision T7910 workstation (Intel®Xeon® Processor E5-2683 v4 with dual processors, 64 cores, and 256 GB RAM).

3. Results and discussion

3.1. Model calibration and validation

The elliptical VCU geometry and polydispersed PSD were employed for the model calibration and validation. The parameters, $F_{i,\text{phase}}$, used in the CFPD model and the parameters, k_{ij} , used in PK model were calibrated and optimized by using the mean values of the benchmark clinical data measured by Heuberger, Guan [17] and the measured puff pattern from Azorlosa, Greenwald and Stitzer [5] (see Table 2 Calibration Case). By fitting the $C_{\text{THC-plasma}}$ profiles (Fig. 4 (a)) with Heuberger, Guan [17], $F_{i,\text{phase}}$ and k_{ij} values were determined via a multiple parameter optimization algorithm employed in existing research [26, 31]. The values of k_{ij} are given in Table 1. The finalized $F_{i,\text{phase}}$ values are listed here, $F_{i,\text{vapor}}$ ($i = 1, 2, 3, 4$) = 0.16, 0.40, 0.60, 0.90 and $F_{i,\text{particle}}$ ($i = 1, 2, 3, 4$) = 0.05, 0.20, 0.30, 0.40.

The CFPD-PK model was validated based on existing benchmark experimental data, i.e., $C_{\text{THC-plasma}}$ vs. time, provided by Perez-Reyes, Owens and Di Guiseppi [13]. As listed in Table 2, the puff information of the validation cases was also based on the work by Refs. [5,13]. The comparison of $C_{\text{THC-plasma}}$ between CFPD-PK and clinical data are shown in Fig. 4 (b). The validation case and data comparisons are also listed in Table 2. The differences in the maximum THC-plasma concentration (C_{max}) and AUCs between the CFPD-PK data and experimental measurements were less than 3.6% and 4.0%, respectively. Therefore, the CFPD-PK model developed in this study was able to accurately predict the $C_{\text{THC-plasma}}$ under specific puffing protocol and THC dosing conditions [5,13].

Table 1
Parameter values in the PK model.

PK Parameter Description	Symbol	Value	Unit
THC transfer rate constant k_{ij} from compartment i to j	k_{12}	1.3	hour ⁻¹
	k_{13}	4.09	hour ⁻¹
	k_{21}	0.039	hour ⁻¹
	k_{31}	1.01	hour ⁻¹
Elimination rate of THC from the central compartment	k_{10}	5.5	hour ⁻¹
Volume of the central compartment	V_1	6.15	liter

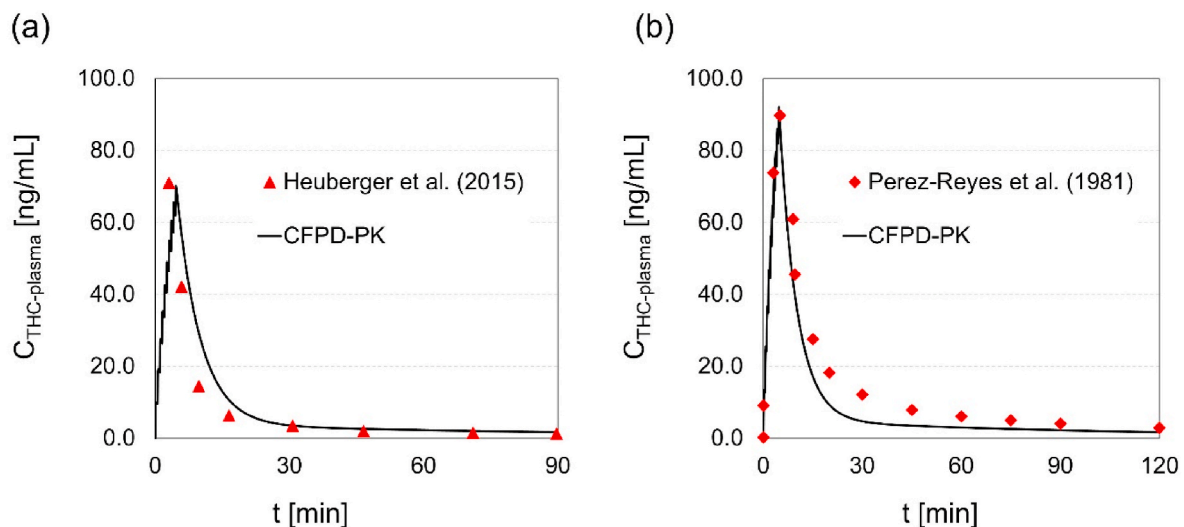


Fig. 4. CFPD-PK model calibration (a) and validation (b): comparison of THC-plasma concentration ($C_{\text{THC-plasma}}$) between simulation results and clinical data by Azorlosa, Greenwald and Stitzer [5], Heuberger, Guan, Oyetayo, Klumbers, Morrison, Beumer, van Gerven, Cohen and Freijer [17], and Perez-Reyes, Owens and Di Guiseppi [13].

Table 2
Model calibration and validation cases setup and corresponding PK results.

Case	Puff Duration [s]	Holding Time [s]	Puff Volume [mL]	THC Dose ^a [mg]	C _{max} [ng/mL]	AUC [ng·min/mL]
Azorlosa, Greenwald and Stitzer [5] and Heuberger, Guan, Oyetao, Klumpers, Morrison, Beumer, van Gerven, Cohen and Freijer [17] ^b	4	10	120	2.0	71.3	677.47
Calibration Case	4	10	120	2.0	70.1	703.39
Perez-Reyes, Owens and Di Guiseppi [13]	1.59 ± 0.54	11.5 ± 2.3	20	8.82	88.3	1105.34
Validation Case	1.6	11.4	20	8.82	92.1	1061.0

^a THC exists in botanical raw materials (BRMs), but not necessarily in the smoke or vapor.

^b The puff pattern data are from Azorlosa, Greenwald and Stitzer [5], and the rest data are from Heuberger, Guan, Oyetao, Klumpers, Morrison, Beumer, van Gerven, Cohen and Freijer [17] (see Section 3.1 for more details).

3.2. Pulmonary airflow fields

To investigate the effects of puff protocols and airway morphologies on the THC transport and translocations, eight cases were selected and simulated. The puffing conditions, geometries, and PSDs employed for each case are listed in Table 3.

Fig. 5 compares the distributions of normalized pressure \tilde{p} and normalized airflow velocity magnitude \tilde{v} for the steady-state inhalation cases between idealized and elliptical VCU geometries in the sagittal plane ($z = 0$ m and $x = 0.0035$ m, respectively). The \tilde{p} and \tilde{v} are calculated based on Eqs. (21) and (22), i.e.,

$$\tilde{p} = \frac{p}{p_{in}} \quad (21)$$

$$\tilde{v} = \frac{v}{v_{in}} \quad (22)$$

where p_{in} and v_{in} are the averaged pressure and velocity magnitude at the mouth inlet, respectively.

Fig. 5 also compares the distributions of normalized pressure and normalized airflow velocity magnitude for the steady-state inhalation cases between idealized and elliptical VCU geometries in the sagittal plane ($z = 0$ m and $x = 0.0035$ m, respectively). Generally, similar pressure and velocity distribution styles can be found between using the idealized geometry and the elliptical VCU geometry, with moderate differences. For the idealized geometry, the high-pressure spot was located at the sublingual region (see Fig. 5 (a)), which was attributed to the impingement effect of the airflow when impacting the high-curvature wall representing the tongue. For the idealized geometry, airflow impingement reached the sublingual area directly and then formulated circulation in the oral cavity (see Fig. 5 (b)). In contrast, the highest pressure was located at the back of the pharynx (see Fig. 5 (a)), which was also the impact point of the inhalation air jet. The airflow impingement hits the posterior of the oropharynx in the elliptical VCU geometry. Fig. 5 (c) shows the iso-surfaces of the velocity magnitude, which demonstrates that the laryngeal jet was more noticeable in idealized geometry compared with the elliptical VCU geometry due to the higher contraction ratio at the glottis. Therefore, the anatomical variability of the upper airway geometry had a noticeable influence on

Table 3
Case setup information for parametric analysis.

Case	Puff Duration [s]	Holding Time [s]	Puff Volume [mL]	THC Dose ^a [mg]	Geometry Model	PSD
Case 1	4	10	120	2.0	Idealized	Monodispersed
Case 2	4	10	120	2.0	Idealized	Polydispersed
Case 3	4	10	120	2.0	Elliptical VCU	Monodispersed
Case 4	4	10	120	2.0	Elliptical VCU	Polydispersed
Case 5	1.6	11.4	20	8.82	Idealized	Monodispersed
Case 6	1.6	11.4	20	8.82	Idealized	Polydispersed
Case 7	1.6	11.4	20	8.82	Elliptical VCU	Monodispersed
Case 8	1.6	11.4	20	8.82	Elliptical VCU	Polydispersed

^a THC are known to be present in the botanical raw material (BRM).

the pulmonary airflow patterns.

Fig. 5 also shows the flow pattern differences associated with different puffing patterns. Specifically, Figs. 5 (a)–(c) present the pressure and velocity distributions at the time close to the end of the two different puff patterns (see Table 2). With higher volumetric flow rates, the jet-induced airflow velocity distributions in Cases 1–4 were more fully developed than Cases 5–8. Accordingly, the vapor and particle transport, absorption, and deposition were all influenced by the different puff volumetric flow rates and durations (see Sections 3.3, 3.4, and 3.5).

3.3. THC vapor transport and absorption

By visualizing the distributions of nondimensionalized vapor mass fraction $\tilde{Y}_{THC,v}$ and mass absorption flux $\tilde{m}_{ab,v}$ in Figs. 6 and 7, the effects of airway anatomy and the puff patterns on lung dosage of the THC vapor are compared. Specifically, the normalized THC vapor mass fraction $\tilde{Y}_{THC,v}$ is defined as

$$\tilde{Y}_{THC,v} = \frac{Y_{THC,v}}{Y_{in,v}} \quad (23)$$

where $Y_{in,v}$ is the vapor THC mass fraction at the mouth inlet.

The normalized mass absorption flux $\tilde{m}_{ab,v}$ is defined as

$$\tilde{m}_{ab,v} = \frac{m''_{ab,v}}{m''_{in,v}} \quad (24)$$

in which $m''_{in,v}$ is the mass flux (kg/m²s) at the mouth inlet.

In general, the THC vapor transport is influenced by both airflow convection and vapor diffusion (see Figs. 6 (a)–(e)). As shown in Figs. 6 (a)–(d), the effects of the upper airway anatomy on the $\tilde{Y}_{THC,v}$ is similar to the airflow velocity distributions. Specifically, with the higher secondary flows in the oral cavity and pharynx of the elliptical VCU model, the dispersion effect of the THC vapor in the oral cavity is more dominant, compared with the more concentrated $\tilde{Y}_{THC,v}$ distributions in the idealized upper airway model. With the more connected and elongated high-velocity jet core in the idealized upper airway model (see Fig. 5 (c) for the jet core comparisons), the high-concentration vapor cores extend further into the trachea in the idealized airway compared with the

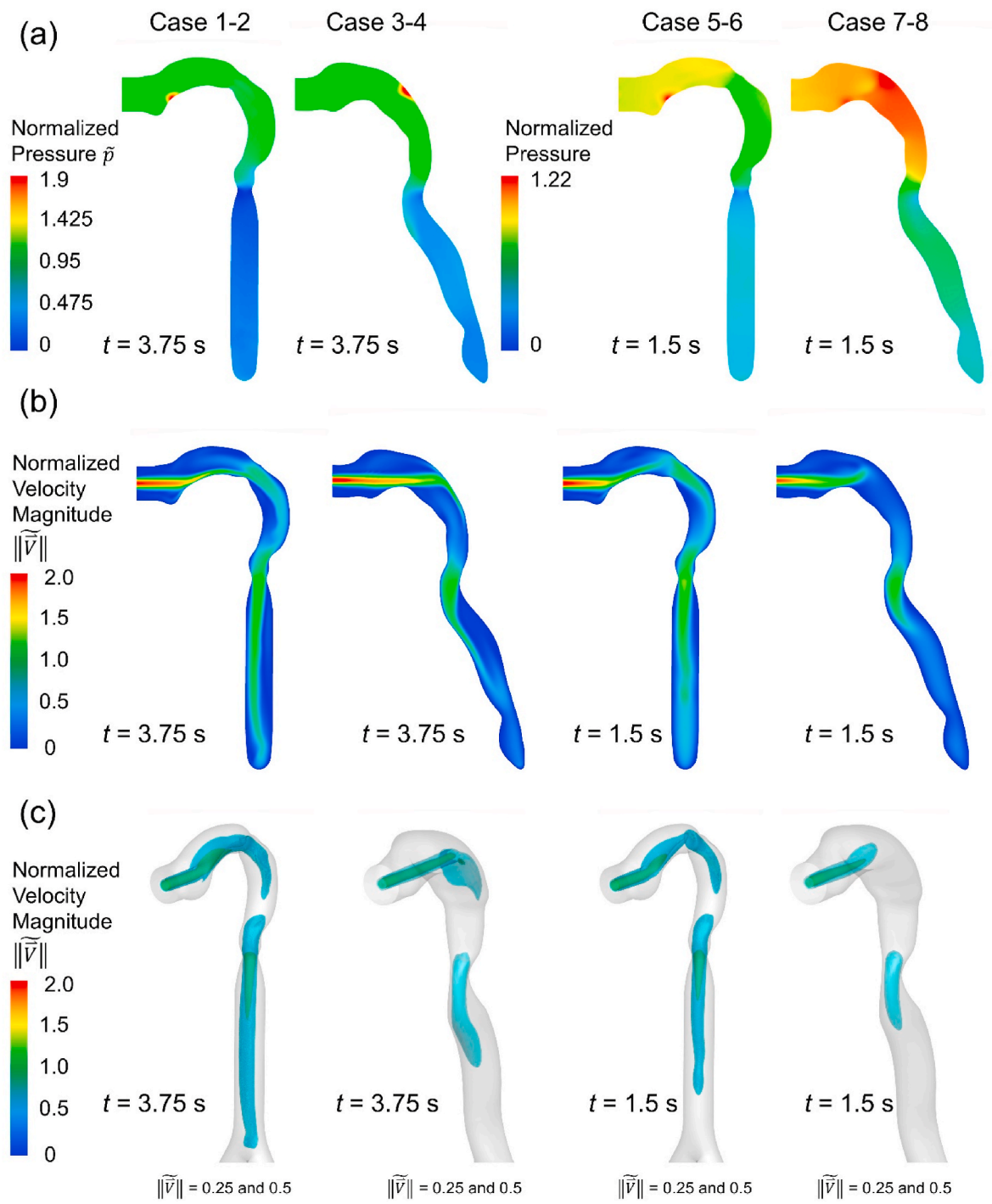


Fig. 5. Comparison of flow patterns among Cases 1 to 8: (a) normalized pressure distribution during steady inhalation at the sagittal plane, (b) normalized velocity magnitude contour at the sagittal plane, and (c) distribution of iso-surfaces of normalized velocity magnitude.

elliptical VCU airway. Furthermore, the intensity of the puff also has a significant influence on the vapor distributions in the upper airways. With the higher inhalation volumetric flow rate and longer puff duration in Cases 1–2, high-concentration $\tilde{Y}_{\text{THC},v}$ the jet core extends further downstream in both airway geometries in Cases 1–2 compared with Cases 3–4 because of the more substantial convection effect. Using Cases 1–2 as an example, Fig. 6 (e) presents the distributions of $\tilde{Y}_{\text{THC},v}$ at different time stations during the puff, which visualizes the progression of the high-concentration vapor jet core from $t = 0.5$ s to $t = 3.0$ s. The $\tilde{Y}_{\text{THC},v}$ distribution was initially increasing and reached the maximum concentration at approximately $t = 1$ s. Afterward, due to the increased

wall absorption flux induced by the high near-wall concentration gradient $\tilde{Y}_{\text{THC},v}$ started to decrease in the oral cavity from $t = 1$ s to $t = 4$ s.

Using Cases 1–4 as examples, Figs. 7 (a) and (b) shows the contours of the normalized THC vapor absorption flux $\tilde{m}_{ab,v}''$ for both airway geometries at different time stations from 1.0 s to 5.0 s, to show the effect of the upper airway anatomy on the localized $\tilde{m}_{ab,v}''$ distributions of the THC vapor. With different upper airway geometries, the differences of $\tilde{m}_{ab,v}''$ distributions between the two airway geometries were found in the oral cavity and the anterior region from the glottis to the trachea.

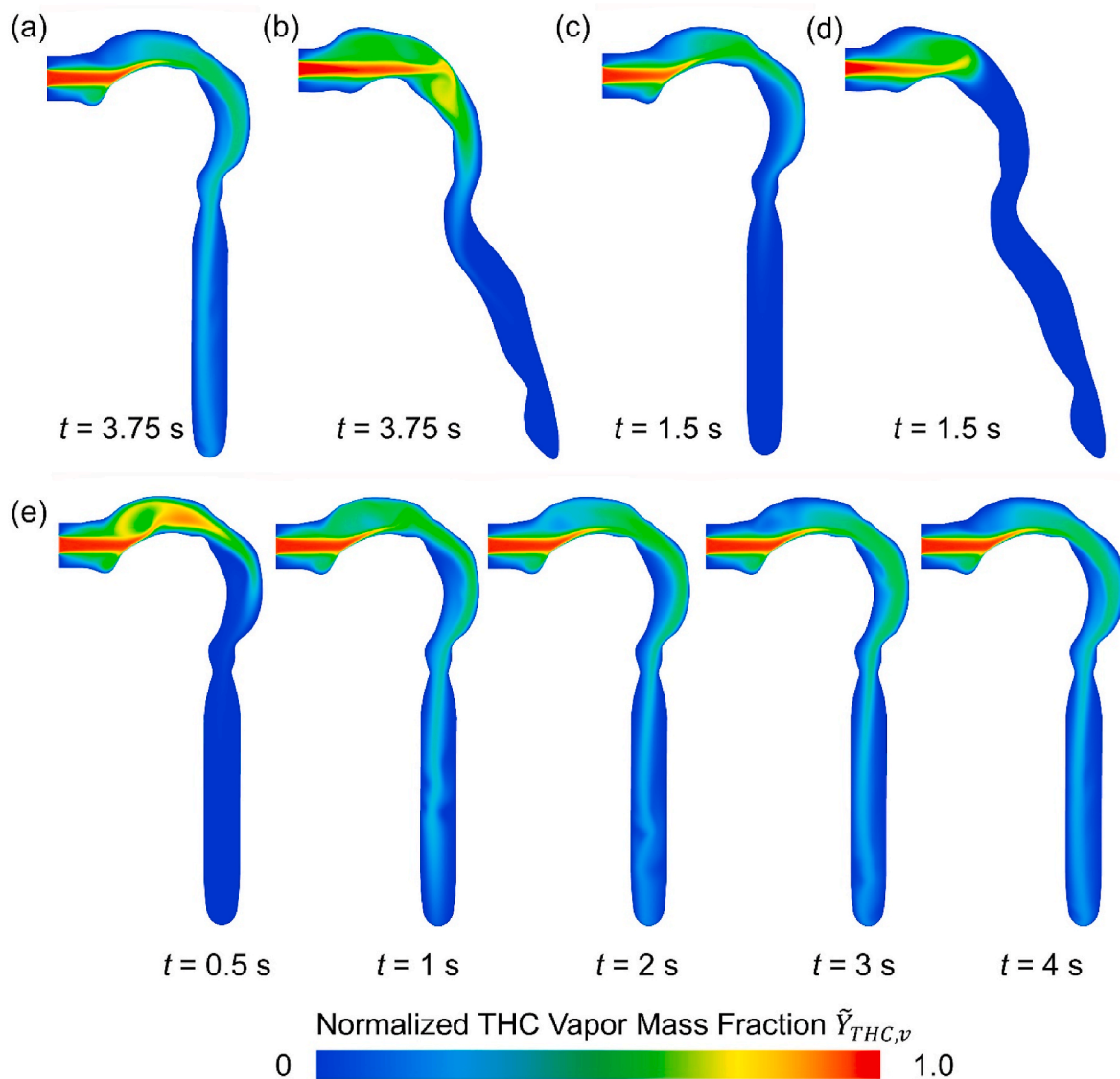


Fig. 6. Normalized THC vapor phase mass fraction distribution during steady inhalation at the sagittal plane in (a) Cases 1–2, (b) Cases 3–4, (c) Cases 5–6, and (d) Cases 7–8, and (e) normalized THC vapor phase mass fraction distribution at different time phases at the sagittal plane in Cases 1–2.

Specifically, during the inhalation, $\tilde{m}_{ab,v}''$ was higher in the mouth-to-throat region of the idealized airway geometry and the throat-trachea region for the elliptical VCU airway case. At $t = 1.0$ s, $\tilde{m}_{ab,v}''$ can reach as high as 0.004 in the almost entire oral cavity for idealized geometry. In contrast, $\tilde{m}_{ab,v}''$ in the oral cavity of the elliptical VCU airway was relatively lower than the idealized airway cases at $t = 1.0$ s, which is because of the different convection effects induced by the different impaction locations of the mouth inlet jets (see Figs. 6 (a) and (b)). Without the impaction in the lower palate, using the elliptical VCU model will have more inhaled vapor directly convected towards the posterior of the oropharynx, which leads to the differences in the $\tilde{m}_{ab,v}''$ distributions at the R1 walls, compared with the idealized airway geometry. The different impaction locations using the two upper airway geometries lead to different high THC absorption rate locations (see the red dash circles at $t = 1.0$ s in Fig. 7 (b)). Another difference occurs at the pharynx and anterior of the trachea region, where $\tilde{m}_{ab,v}''$ was higher in the elliptical VCU geometry compared with idealized airway geometry. The difference in the $\tilde{m}_{ab,v}''$ distribution at the trachea was mainly due to the different dispersion characteristics induced by the different secondary

flow patterns, as well as the impinging locations of the laryngeal jets (see Figs. 6 (a) and (b)). Indeed, the high $\tilde{m}_{ab,v}''$ region at the anterior of the trachea in the elliptical VCU airway geometry (see the top solid circle at $t = 2.0$ s in Fig. 7 (b)) was the direct result of laryngeal jet impingement, which does not exist in the idealized airway geometry (see Fig. 7 (a)). Another difference resulted from the distinct laryngeal jet core topologies is marked by the bottom red circle at $t = 2.0$ s in Fig. 7 (b). Compared with the $\tilde{m}_{ab,v}''$ distribution near the carina between the two airway geometries, $\tilde{m}_{ab,v}''$ distribution was more evenly distributed and higher in the idealized airway geometry. Based on the above-mentioned differences in $\tilde{m}_{ab,v}''$ distributions, the upper airway anatomy had a noticeable influence on the local vapor absorption flux distributions.

To further investigate how the puff pattern can influence the regional vapor absorption, Figs. 8 (a)–(d) show the transient regional absorption rates $\dot{m}_{ab,v}$ (ng/s) of THC vapor in different regions (see Fig. 1), while Table 4 lists the regional and total accumulated absorption masses $m_{ab,v}$ (ng) at the end of one puff cycle for Cases 1–8. With the longer puff duration and higher inhaled volumetric flow rate, the regional $\dot{m}_{ab,v}$ were more evenly distributed in Cases 1–4 (see Figs. 8 (a) and (b))

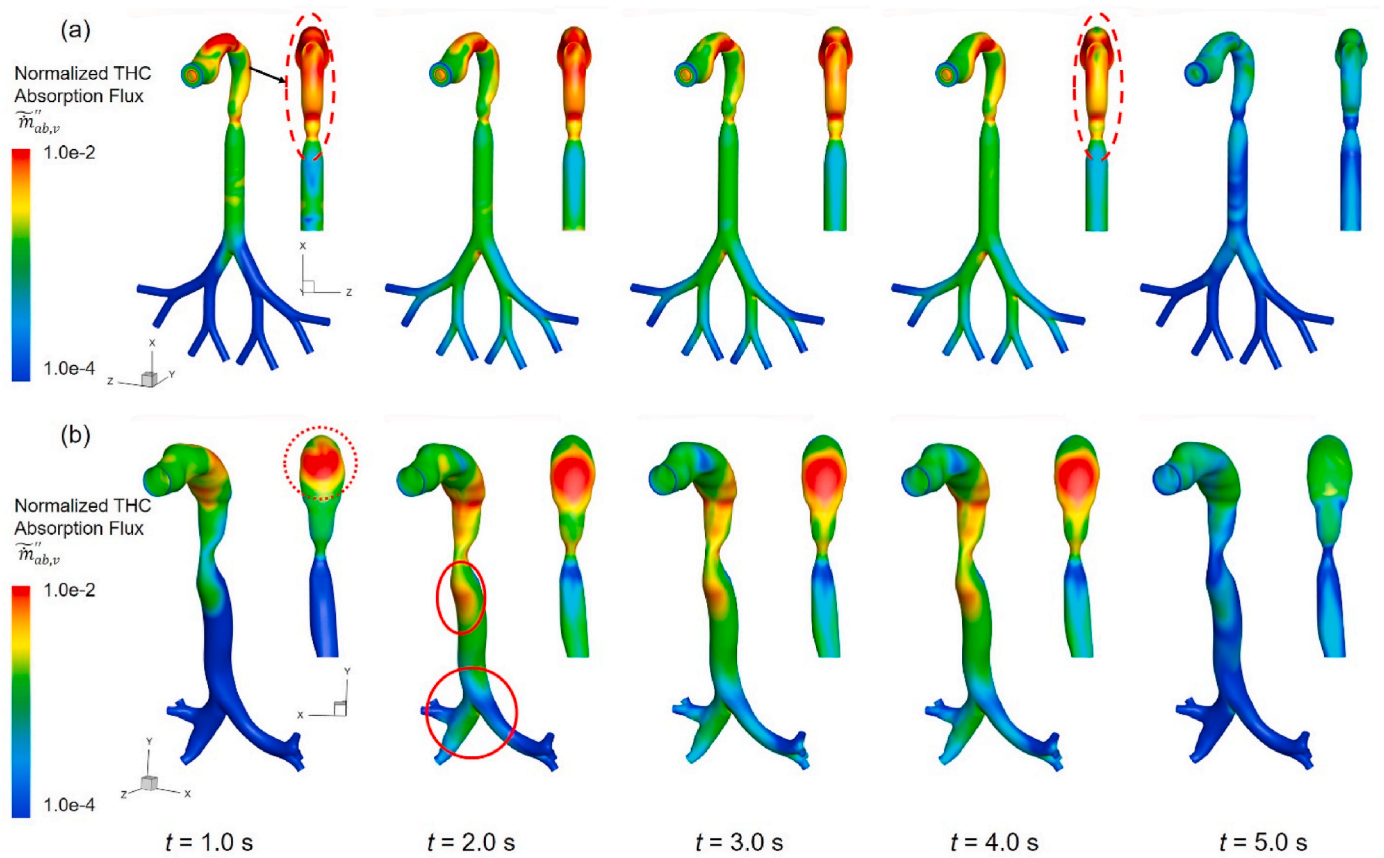


Fig. 7. Comparison of normalized THC absorption flux at different time stations by upper airway between two geometries in Cases 1–4: (a) idealized (Cases 1 & 2) and (b) elliptical VCU (Cases 3 & 4). High THC absorption rate locations are denoted in the red circles.

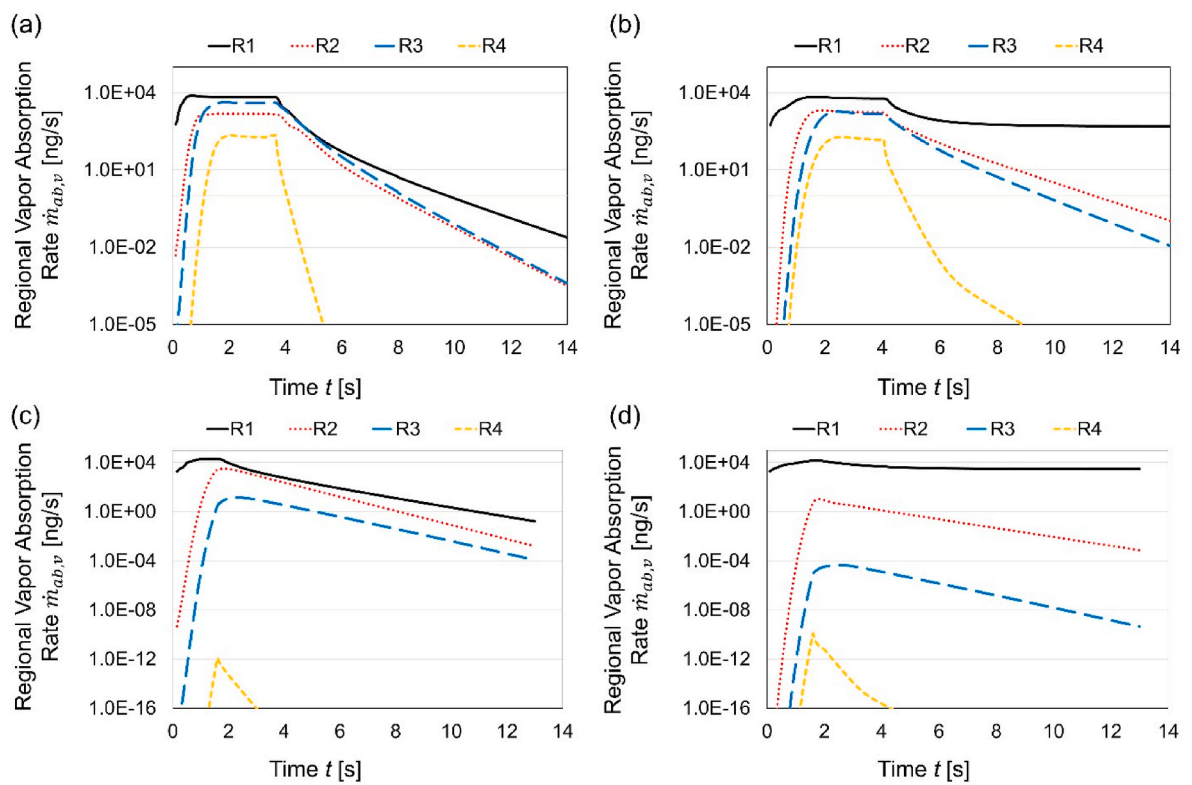


Fig. 8. Accumulated THC vapor absorption in regions R1 to R4 during one puff: (a) Cases 1–2, (b) Cases 3–4, (c) Cases 5–6, and (d) Cases 7–8.

Table 4

Accumulated THC vapor absorption masses $m_{ab,y}$ in different regions at the end of one puff cycle.

	R1 (ng)	R2 (ng)	R3 (ng)	R4 (ng)	Total (ng)
Cases 1–2	1.31E+03	2.56e+02	6.03e+02	2.20e+01	2.19e+03
Cases 3–4	1.49E+03	3.05e+02	2.26e+02	1.91e+01	2.04e+03
Cases 5–6	1.68E+03	2.08e+02	1.26e+00	8.99e-15	1.88e+03
Cases 7–8	3.14E+03	6.43e-01	4.17e-06	7.92e-13	3.14e+03

compared with Cases 5–8 (see Figs. 8 (c) and (d)). Specifically, the long and strong puff employed in Cases 1–4 can effectively carry inhaled THC vapors to downstream regions (i.e., R3 and R4), while the short and mild puff used in Cases 5–8 was not able to bring THC vapors to R4. Such a difference led to the negligible absorption rate in R4 (see Figs. 8 (c) and (d)). The comparison indicates that, if the delivery of THC to the distal lung is preferred, long and strong puff should be recommended. It is also worth mentioning that the upper airway anatomy effect on the regional absorption rate distributions was significant in Cases 5–8, with the short and mild puff. Data of the accumulated absorption masses shown in Table 4 also support the above-mentioned discussion. Another interesting finding indicated by Table 4 is that the values of 8.99e-15 and 7.92e-13 ng are due to numerical/floating-point errors because fundamentally one molecule has a mass in the range of 1e-13 ng.

3.4. THC particle transport and deposition

Comparisons of localized particle deposition patterns at the end of

breath-holding after the first puff among cases are shown in Fig. 9. Particles are colored based on their residence time or diameters, ranging from 226 to 972 nm. The deposition patterns using the monodispersed PSDs (Cases 1, 3, 5, and 7) were visually noticeable in the cases using realistic polydispersed particle size distributions (Cases 2, 4, 6, and 8). Specifically, the deposition of large particles ($d_p > 500$ nm) in polydispersed cases concentrated at the mouth-to-throat region, as shown in the red circles, which were not found in the monodispersed cases with more scattered deposition patterns. In addition, large particles deposited at the bronchi region (see red dash circle in Fig. 9 for Case 2 and Case 4). In contrast, the deposition of small particles ($d_p < 400$ nm) were few, indicating that most of the small particles entered the deeper lung ($>G4$). Furthermore, with the shorter puff duration and lower puff volumetric flow rate (see Table 3 for puff protocol data), the deposition of the particles is restricted from mouth to G1 in the idealized airway (Cases 5–6), while from mouth to glottis in the elliptical VCU airway (Cases 7–8). The deposition of particles in Cases 1–4 spread across all regions in the two upper airway geometries. The deposition differences indicate that a long and strong puff led to the THC particle deposition in the deeper lung, which may enhance the therapeutic effect and the potential safety issues if the delivered dose is not controlled well. Deposition patterns in Cases 7–8 resulted from the more substantial recirculating flows in the oral cavity of the elliptical VCU airway, which made the traveling time of particles in the oral cavity longer than the idealized upper airway, with a higher chance to deposit in the same region. The deposition pattern differences shown in Cases 5–8 proved that the subject variabilities of the upper airway anatomy could significantly influence the THC particle deposition.

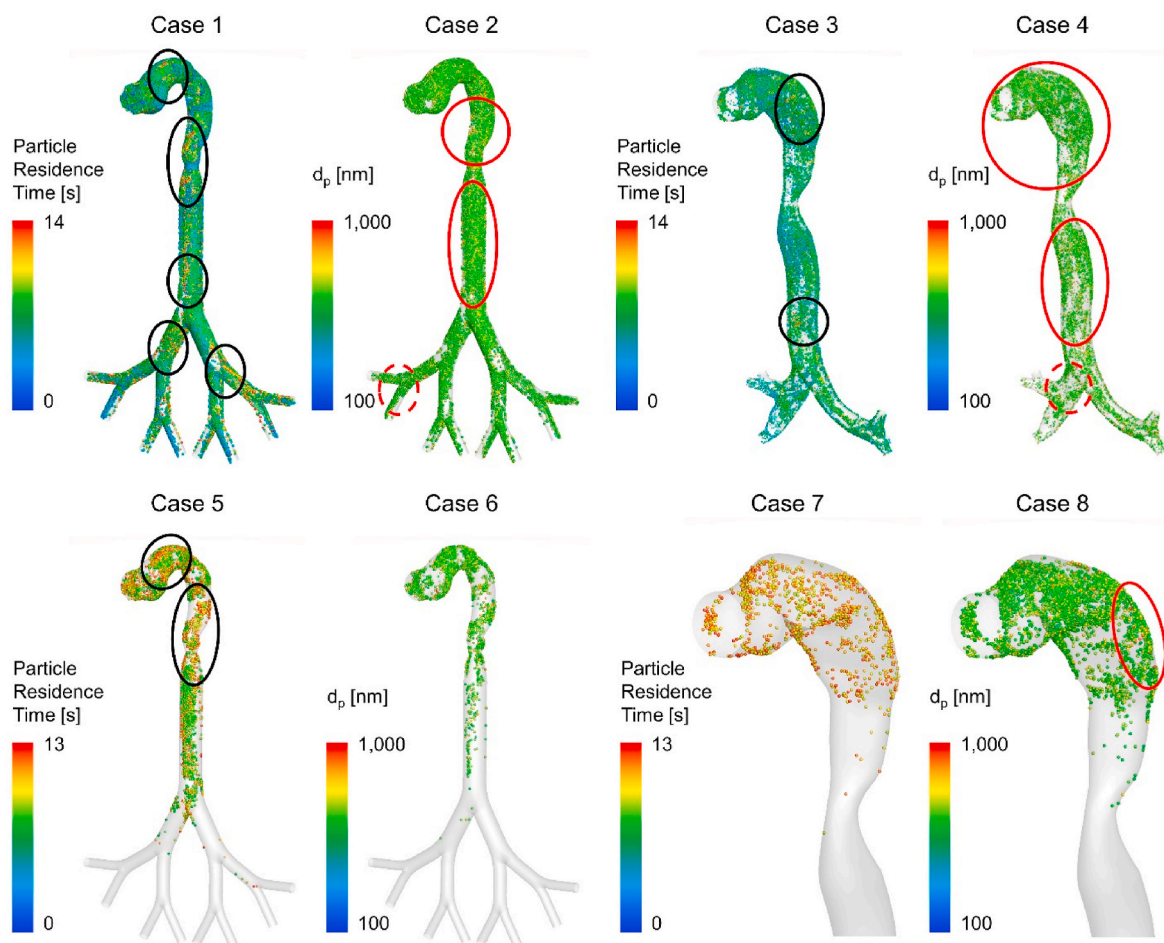


Fig. 9. Deposition distribution of particles colored with particle residence time and diameter size d_p in upper airway at the end of the holding after a single puff. Large particle ($D_p > 500$ nm) deposition locations are denoted in red circles. Particles with long residence time (>10 s) are denoted in black circles.

Fig. 10 (a) and (b) compare the regional and total deposition fractions (DFs) of THC particles in different regions of Cases 1 to 8. The particle depositions in G1 and G2 were less noticeable compared with the particle depositions in other regions. Differences in regional deposition fractions and the total particle mass deposited were observed between using the idealized upper airway and elliptical VCU airway. The Elliptical VCU airway provided lower total deposition than the idealized upper airway (see quantitative comparisons in the next paragraph). Higher RDF at the mouth-throat region in Cases 1 and 5 compared with Cases 3 and 7 is because of the higher curvature of the mouth-throat region, which prevents the particle from transporting into deeper lung. Thus, subject-specific upper airway geometry should be used to account for the inter-subject variability effect on the CFPD prediction accuracies. For the comparisons between monodispersed and polydispersed cases, Fig. 9 indicates that monodispersed PSD overestimated particle deposition fraction and deposition mass for both idealized and elliptical VCU cases. Therefore, using the simplified monodispersed PSDs, the CFPD model was not able to accurately predict the local and regional depositions compared with using the realistic polydispersed particle distributions. The realistic particle sizes need to be accurately considered in the CFPD simulations. Furthermore, with a similar holding time, the puff duration and puff volumetric flow rate had a noticeable effect on particle deposition. Specifically, Cases 1–4 had much higher particle deposition masses than Cases 5–8, which indicated that the stronger inertial impaction of the stronger and longer puff leads to more particle depositions.

Furthermore, Figs. 11 (a) and (b) visualized the transient particle deposition (i.e., absorption in general) rate $\dot{m}_{ab,p}$ (ng/s) vs. time. The effect of upper airway anatomy on particle deposition was not significant with the puff protocol used in Cases 1–4 (see Fig. 11 (a)) since the difference in the total $m_{ab,p}$ of one puff between Cases 1 and 3 was less than 22.1%. However, the anatomical effect becomes more noticeable with the short and mild puff used in Cases 5–8 (see Fig. 11 (b)) as the difference in the total $m_{ab,p}$ over one puff between Cases 5 and 7 was

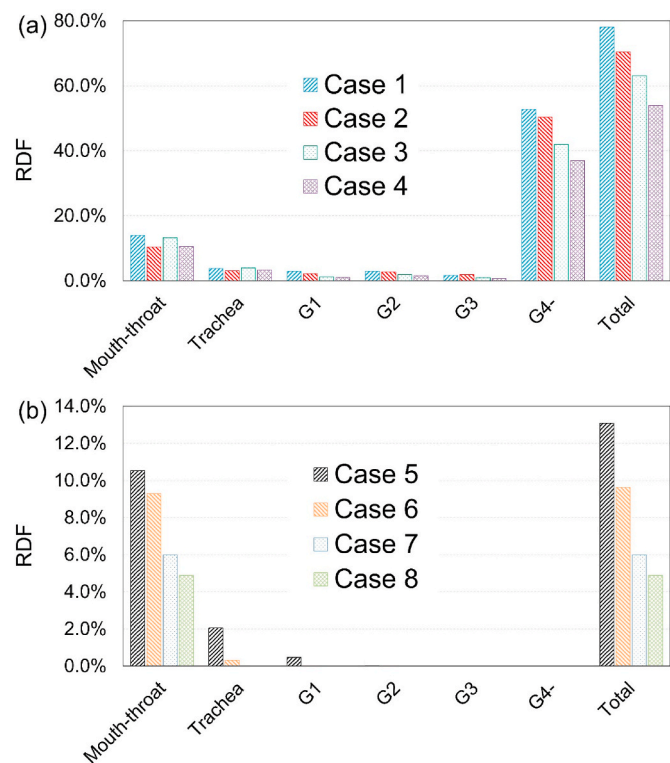


Fig. 10. Comparison of regional depositions of THC particles: (a) Cases 1–4 (b) Cases 5–8.

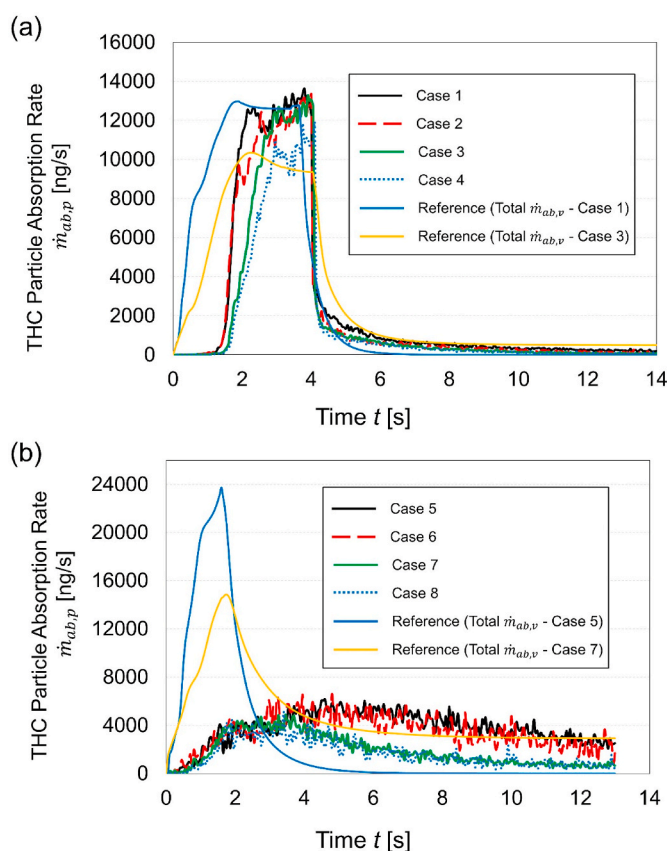


Fig. 11. Accumulated THC particle deposition mass during one puff: (a) Cases 1–4, and (b) Cases 5–8.

approximately 37.5%. Furthermore, with the short and mild puff used in Cases 5–8 (see Fig. 11 (b)), the total accumulated particle deposition masses lower than the accumulated vapor absorption masses, compared with Cases 1–4 (see Fig. 11 (a)).

3.5. THC pharmacokinetics (PKs)

Associated with different airway geometries and puff patterns, the PK profiles $C_{THC-plasma}$ s are visualized in Figs. 12 (a) and (b), with 8 consecutive puffs and the following 60-minute duration. The concentration peak values C_{max} (ng/mL) and AUCs (ng/mL-min) are listed in Table 5. Specifically, the PK data which are shown in Fig. 12 and Table 5 indicate the findings:

- (1) With the same puff protocol and THC dose, the PK profiles between the monodispersed and polydispersed cases were similar (see Fig. 12 (a) and (b)). The similarity was attributed to the relatively low deposition mass rate of the particle phase compared with the relatively high vapor absorption rate, especially for Cases 5–8 (see Figs. 11 (a) and (b)). For example, in Cases 7 and 8, the absorption mass $m_{ab,p}$ of THC particles (see the area under curve in Fig. 11) was less than 30% compared with the accumulated $m_{ab,v}$ of the THC vapor during a single puff.
- (2) With the same puff protocol and inhaled THC dose (see Table 3), the idealized upper airway cases predicted higher $C_{THC-plasma}$ profiles than the elliptical VCU airway cases. For Cases 1–4, such observations were due to higher particle depositions and vapor absorptions using the idealized airway than the elliptical VCU airway (see Fig. 10 and Table 4). For Cases 5–8, although the accumulated total $m_{ab,v}$ over one puff using the elliptical VCU airway was 40.1% more than the idealized upper airway (see

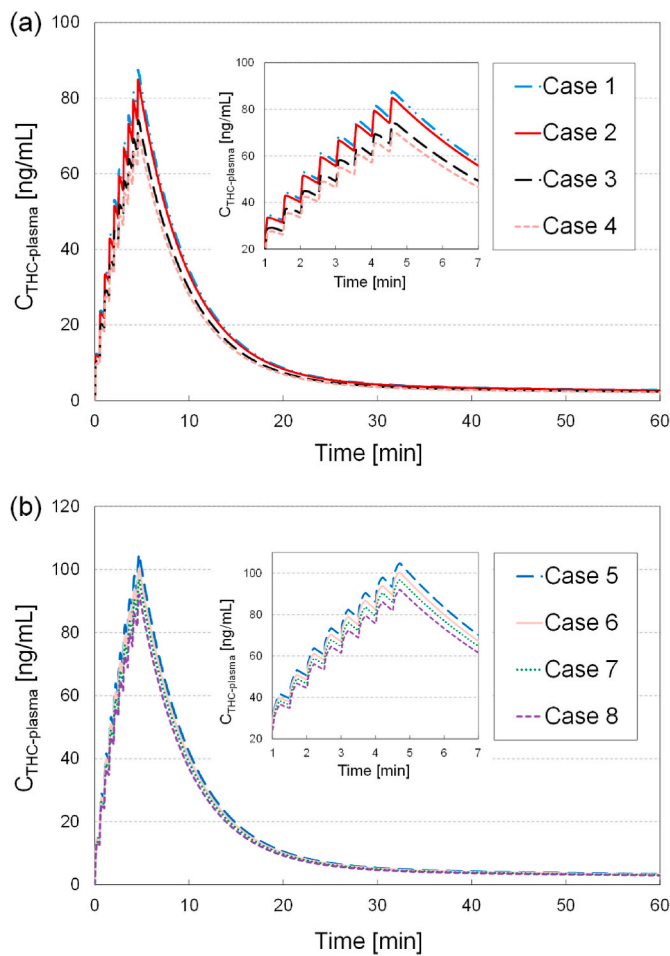


Fig. 12. Comparisons of $C_{THC-plasma}$ after 8 puffs within 1 h: (a) Cases 1–4, (b) Cases 5–8.

Table 5
Comparisons of C_{max} and AUC data for Cases 1–8.

Case	C_{max} [ng/mL]	AUC (60 min) [(ng/mL)·min]
Case 1	87.5	871.8
Case 2	84.9	844.1
Case 3	64.5	744.0
Case 4	61.7	703.4
Case 5	104.9	1056.0
Case 6	100.5	1012.8
Case 7	96.8	973.4
Case 8	92.1	926.6

Table 4), higher particle absorption profile using the idealized upper airway (see Fig. 11 (b)) resulted in the total THC particle-vapor absorption rate higher than the elliptical VCU airway, which still led to a higher PK profile using the idealized upper airway than the elliptical VCU airway.

(3) In addition, it is worth mentioning that C_{max} and AUC values Cases 5–8 were higher than Cases 1–4 (see Table 5). This is because that although the puff is short and mild in Cases 5–8 compared with Cases 1–4, the total inhaled THC dose, i.e., 8.82 mg for Cases 5–8 is much higher than 2.0 mg for Cases 1–4.

4. Conclusions

In the present study, an experimentally calibrated and validated CFPD-PK model has been developed to predict the transport, deposition,

absorption, and translocation of the inhaled THC particle-vapor mixtures. The simulation results permit three major conclusions, i.e.,

- (1) Although using the simplified monodispersed PSD led to a visually noticeable difference in the THC particle deposition prediction than using the realistic polydispersed PSD, the differences in the PK profile predictions were less noticeable, which is because the THC vapor absorption mass was 1.3–3.1 times higher than the THC particle absorption mass.
- (2) With a short and mild puff, the effects of upper airway anatomy were significant on vapor and particle deposition predictions, as well as the PK profile predictions. Therefore, the subject-specific upper airway geometry was needed in the CFPD-PK simulation to capture the effect of the inter-subject variability in airway anatomy accurately.
- (3) Longer puff duration and higher puff volumetric flow rates led to higher THC delivery efficiency to the deeper lung than shorter puff duration and lower puff volumetric flow rates. Such findings indicate that the THC delivery to the deeper lung is essential for specific treatments. For example, when using inhalation therapy to deliver THC for pain relief [53], long and strong puffs should be considered.

In summary, the CFPD-PK model developed in this study provides helpful insights into the deposition and absorption of smoked and vaporized cannabis under different puff protocols and dosing scenarios. The modeling framework has the potential to provide novel insights to form the basis for the development and assessment of proposed cannabis drug products containing THC. With appropriate validations and verifications, the CFPD-PK model can be refined and employed for research related to formulations, dosing, potency, and physicochemical behaviors of other inhaled therapeutic aerosols.

5. Limitations of the present study and future work

As the limitations of this numerical study, the assumptions and simplifications are:

- (1) The hygroscopicity of the THC particles in the airway during their transport is neglected, and the air humidity effect on $D_{THC-air}$ is neglected. The effect of condensation and evaporation between the THC particles and the water vapor in human respiratory systems will be integrated using the existing method [25,32].
- (2) The metabolism of THC in lung tissue was not considered and will be considered in the next-generation CFPD-PK model by revising the governing equations in Section 2.2.3.
- (3) Only two puff protocols were employed in this study, focusing on the influence of puffing intensity and duration, but not considering the effects of holding duration and exhalation pattern. The effects of holding duration and exhalation pattern will be investigated by employing more puff protocols in the future.
- (4) Only two upper airway geometries were used to investigate the inter-subject variability effect on THC transport, deposition, absorption, and translocation, which will be expanded to guarantee the statistical robustness via adopting additional upper airway geometries [43].
- (5) The 1st-order boundary condition for vapor absorption at the airway wall was employed, instead of higher-order boundary conditions [54].
- (6) The hypothesis that THC has different absorption rate in different lung regions are based on the fact that THC is highly lipophilic like nicotine. The hypothesis needs to be tested using experiments soon.

Disclaimer

The findings and conclusions in this report have not been formally disseminated by the Food and Drug Administration and should not be construed to represent any Agency determination or policy. The mention of commercial products, their sources, or their use in connection with material reported herein is not to be construed as either an actual or implied endorsement of such products by the Department of Health and Human Services.

Declaration of competing interest

None.

Acknowledgement

The use of Ansys software (Canonsburg, PA) as part of the Ansys-OSU academic partnership agreement is gratefully acknowledged (Dr. Thierry Marchal, Global Industry Director). Part of this research was supported in part by appointment to the Research Participation Program at the Center for Drug Evaluation and Research administered by the Oak Ridge Institute for Science and Education through an interagency agreement between the U.S. Department of Energy and the U.S. Food and Drug Administration.

References

- G. Appendino, A. Minassi, O. Tagliatalata-Scafati, Recreational drug discovery: natural products as lead structures for the synthesis of smart drugs, *Nat. Prod. Rep.* 31 (7) (2014) 880–904.
- W. Hall, M. Lynskey, Assessing the public health impacts of legalizing recreational cannabis use: the US experience, *World Psychiatr.* 19 (2) (2020) 179–186.
- P. Sharma, P. Murthy, M.M.S. Bharath, Chemistry, metabolism, and toxicology of cannabis: clinical implications, *Iran. J. Psychiatry* 7 (4) (2012) 149–156.
- M. Perez-reyes, Marijuana smoking: factors that influence the bioavailability of tetrahydrocannabinol, in: *Research Findings on Smoking of Abused Substances*, 1990, pp. 42–62.
- J.L. Azorlosa, M.K. Greenwald, M.L. Stitzer, Marijuana smoking: effects of varying puff volume and breathhold duration, *J. Pharmacol. Exp. Therapeut.* 272 (2) (1995) 560.
- M. Huestis, Pharmacokinetics of THC in inhaled and oral preparations, in: G. G. Nahas, et al. (Eds.), *Marihuana and Medicine*, Humana Press, Totowa, NJ, 1999, pp. 105–116.
- J.-E. Lindgren, et al., Clinical effects and plasma levels of Δ^9 -Tetrahydrocannabinol (Δ^9 -THC) in heavy and light users of cannabis, *Psychopharmacology* 74 (3) (1981) 208–212.
- R.G. Pertwee, in: *Cannabinoids*, R.G. Pertwee (Eds.), Pharmacological Actions of Cannabinoids, Springer Berlin Heidelberg, Berlin, Heidelberg, 2005, pp. 1–51.
- L.J. McBurney, B.A. Bobbie, L.A. Sepp, GC/MS and EMIT Analyses for Δ^9 -tetrahydrocannabinol Metabolites in Plasma and Urine of human subjects, *J. Anal. Toxicol.* 10 (2) (1986) 56–64.
- T.R. Spindle, et al., Acute effects of smoked and vaporized cannabis in healthy adults who infrequently use cannabis: a crossover trial, *JAMA Netw. Open* 1 (7) (2018) e184841–e184841.
- C. Lanz, et al., Medicinal cannabis: in vitro validation of vaporizers for the smoke-free inhalation of cannabis, *PLoS One* 11 (1) (2016) e0147286–e0147286.
- D. Gieringer, Cannabis "vaporization": a promising strategy for smoke harm reduction, *J. Cannabis Ther.* 1 (2001).
- M. Perez-Reyes, S.M. Owens, S. Di Guiseppi, The clinical pharmacology and dynamics of Marihuana cigarette smoking, *J. Clin. Pharmacol.* 21 (S1) (1981) 201S–207S.
- P. Pol, et al., Cross-sectional and prospective relation of cannabis potency, dosing and smoking behaviour with cannabis dependence: an ecological study, *Addiction* 109 (7) (2014) 1101–1109.
- E.A. McClure, M.L. Stitzer, R. Vandrey, Characterizing smoking topography of cannabis in heavy users, *Psychopharmacology* 220 (2) (2012) 309–318.
- S. Niedbala, et al., Passive cannabis smoke exposure and oral fluid testing, *J. Anal. Toxicol.* 28 (7) (2004) 546–552.
- J.A.A.C. Heuberger, et al., Population pharmacokinetic model of THC integrates oral, intravenous, and pulmonary dosing and characterizes short- and long-term pharmacokinetics, *Clin. Pharmacokinet.* 54 (2) (2015) 209–219.
- A. Marsot, et al., Population pharmacokinetics model of THC used by pulmonary route in occasional cannabis smokers, *J. Pharmacol. Toxicol. Methods* 85 (2017) 49–54.
- C.C. Hunault, et al., Disposition of smoked cannabis with high Δ^9 -tetrahydrocannabinol content: a kinetic model, *Toxicol. Appl. Pharmacol.* 246 (3) (2010) 148–153.
- Z. Liu, J.H. Martin, Gaps in predicting clinical doses for cannabinoids therapy: overview of issues for pharmacokinetics and pharmacodynamics modelling, *Br. J. Clin. Pharmacol.* 84 (11) (2018) 2483–2487.
- J.T. Leuschner, et al., Pharmacokinetics of delta 9-tetrahydrocannabinol in rabbits following single or multiple intravenous doses, *Drug Metabol. Dispos.* 14 (2) (1986) 230.
- C. Kleinstreuer Feng, A. Rostami, Evaporation and condensation of multicomponent electronic cigarette droplets and conventional cigarette smoke particles in an idealized G3–G6 triple bifurcating unit, *J. Aerosol Sci.* 80 (2015) 58–74.
- Feng, et al., Computational transport, phase change and deposition analysis of inhaled multicomponent droplet–vapor mixtures in an idealized human upper lung model, *J. Aerosol Sci.* 96 (2016) 96–123.
- Feng, et al., An in silico subject-variability study of upper airway morphological influence on the airflow regime in a tracheobronchial tree, *Bioengineering* 4 (4) (2017) 90.
- X. Chen, et al., Numerical investigation of the interaction, transport and deposition of multicomponent droplets in a simple mouth-throat model, *J. Aerosol Sci.* 105 (2017) 108–127.
- A. Haghnegahdar, et al., Development of a hybrid CFD-PBPK model to predict the transport of xenon gas around a human respiratory system to systemic regions, *Heliyon* 5 (4) (2019) e01461–e01461.
- P.G. Koullapis, et al., Particle deposition in a realistic geometry of the human conducting airways: effects of inlet velocity profile, inhalation flowrate and electrostatic charge, *J. Biomech.* 49 (11) (2016) 2201–2212.
- P.G. Koullapis, L. Nicolaou, S.C. Kassinos, In silico assessment of mouth-throat effects on regional deposition in the upper tracheobronchial airways, *J. Aerosol Sci.* 117 (2018) 164–188.
- P. Koullapis, et al., Regional aerosol deposition in the human airways: the SimInhale benchmark case and a critical assessment of in silico methods, *Eur. J. Pharmaceut. Sci.* 113 (2018) 77–94.
- S.D. Dave, A novel hybrid CFD-PBPK model predicting lung-aerosol transport, deposition and species-mass transfer to systemic regions, in: *Mechanical Engineering*, North Carolina State University, 2020.
- A. Haghnegahdar, et al., Computational analysis of deposition and translocation of inhaled nicotine and acrolein in the human body with E-cigarette puffing topographies, *Aerosol. Sci. Technol.* 52 (5) (2018) 483–493.
- Y. Feng, et al., Computational transport, phase change and deposition analysis of inhaled multicomponent droplet–vapor mixtures in an idealized human upper lung model, *J. Aerosol Sci.* 96 (2016) 96–123.
- J. Xi, P.W. Longest, Transport and deposition of micro-aerosols in realistic and simplified models of the oral airway, *Ann. Biomed. Eng.* 35 (4) (2007) 560–581.
- R.L. Walenga, G. Tian, P. Worth Longest, Development of characteristic upper tracheobronchial airway models for testing pharmaceutical aerosol delivery, *J. Biomech. Eng.* 135 (9) (2013).
- P. Bäckman, et al., Advances in experimental and mechanistic computational models to understand pulmonary exposure to inhaled drugs, *Eur. J. Pharmaceut. Sci.* 113 (2018) 41–52.
- N.R. Labiris, M.B. Dolovich, Pulmonary drug delivery. Part I: physiological factors affecting therapeutic effectiveness of aerosolized medications, *Br. J. Clin. Pharmacol.* 56 (6) (2003) 588–599.
- J.V. Fahy, B.F. Dickey, Airway mucus function and dysfunction, *N. Engl. J. Med.* 363 (23) (2010) 2233–2247.
- T.R. Sosnowski, M. Odziomek, Particle size dynamics: toward a better understanding of electronic cigarette aerosol interactions with the respiratory system, *Front. Physiol.* 9 (2018), 853–853.
- A. Haghnegahdar, et al., Computational Analysis of Deposition and Translocation of Inhaled Nicotine and Acrolein in the Human Body with E-Cigarette Puffing Topographies, vol. 52, 2018, pp. 483–493 (5).
- S.J. Heishman, M.L. Stitzer, J.E. Yingling, Effects of tetrahydrocannabinol content on marijuana smoking behavior, subjective reports, and performance, *Pharmacol. Biochem. Behav.* 34 (1) (1989) 173–179.
- E.N. Fuller, P.D. Schettler, J.C. Giddings, New method for prediction of binary gas-phase diffusion coefficients, *Ind. Eng. Chem.* 58 (5) (1966) 18–27.
- M. Tang, R. Cox, M. Kalberer, Compilation and evaluation of gas phase diffusion coefficients of reactive trace gases in the atmosphere: volume 1. Inorganic compounds, *Atmos. Chem. Phys.* 14 (17) (2014) 9233–9247.
- Feng, et al., An in silico inter-subject variability study of extra-thoracic morphology effects on inhaled particle transport and deposition, *J. Aerosol Sci.* 123 (2018) 185–207.
- S.A. Morsi, A.J. Alexander, An investigation of particle trajectories in two-phase flow systems, *J. Fluid Mech.* 55 (2) (1972) 193–208.
- A. Li, G. Ahmadi, Deposition of aerosols on surfaces in a turbulent channel flow, *Int. J. Eng. Sci.* 31 (3) (1993) 435–451.
- P.G. Saffman, The lift on a small sphere in a slow shear flow, *J. Fluid Mech.* 22 (2) (1965) 385–400.
- R. Clift, J.R. Grace, M.E. Weber, *Bubbles, Drops, and Particles*, Academic Press, 1978.
- M.D. Allen, O.G. Raabe, Slip correction measurements of spherical solid aerosol particles in an improved millikan apparatus, *Aerosol. Sci. Technol.* 4 (3) (1985) 269–286.
- F.C. Hiller, et al., Concentration and particle size distribution in smoke from marijuana cigarettes with different Δ^9 -tetrahydrocannabinol content, *Fund. Appl. Toxicol.* 4 (3, Part 1) (1984) 451–454.
- H. Corwin, et al., *Exploring QSAR: Hydrophobic, Electronic, and Steric Constants*. ACS Professional Reference Book, American Chemical Society, 1995.

- [51] Z. Zhang, C. Kleinstreuer, S. Hyun, Size-change and deposition of conventional and composite cigarette smoke particles during inhalation in a subject-specific airway model, *J. Aerosol Sci.* 46 (2012) 34–52.
- [52] W. Hayduk, H. Laudie, Prediction of diffusion coefficients for nonelectrolytes in dilute aqueous solutions, *AIChE J.* 20 (3) (1974) 611–615.
- [53] X. Li, et al., The effectiveness of self-directed medical cannabis treatment for pain, *Compl. Ther. Med.* 46 (2019) 123–130.
- [54] G. Tian, P.W. Longest, Development of a CFD boundary condition to model transient vapor absorption in the respiratory airways, *J. Biomech. Eng.* 132 (5) (2010).